Astron. Astrophys. 326, 203–210 (1997)

ASTRONOMY AND ASTROPHYSICS

Non-linear models for the pulsating post-AGB star SAO 96709: metallic lines

L. Jeannin[1], **A.B. Fokin**[1,2], **D. Gillet**[3], **and I. Baraffe**[1]

[1] Centre de Recherche Astronomique de Lyon (UMR 5574, CNRS), Ecole Normale Supérieure de Lyon, 46 allée d'Italie, F-69364 Lyon Cedex 07, France
[2] Institute of Astronomy of the Russian Academy of Sciences, 48 Pjatnitskaya Str., Moscow 109017 Russia
[3] Observatoire de Haute-Provence, CNRS, F-04870 Saint Michel l'Observatoire, France

Received 27 February 1997 / Accepted 21 April 1997

Abstract. We have performed a set of nonlinear pulsating models for post-AGB stars and have reconstructed the spectral lines for two chemical elements (Ba II, C I). The present analysis is devoted to the interpretation of recent spectroscopic observations of the pulsating post-AGB star SAO 96709. We confirm our earlier result (Jeannin et al. 1996) that the dominant pulsation mode is the first overtone and find an increase of the second overtone in the Fourier spectrum with decreasing mass and metallicity Z. The Doppler velocities deduced from the theoretical line profiles vary from 10 to 15 km.s^{-1} and are in a good agreement with observations. In order to reproduce the observed line broadening, a very large microturbulent velocity has to be introduced, probably with some variations during the pulsational cycle.

Key words: stars: oscillations – stars: post-AGB – shock waves – turbulence – stars: SAO 96709

1. Introduction

Observations of pulsation properties and atmospheric dynamics of post-AGB stars, though difficult due to a relatively small number of objects, provide an excellent tool for their understanding. Due to our poor knowledge of the previous phase of evolution on the Asymptotic Giant Branch and of the so-called superwind phase their very properties cannot be determined on the base of stellar evolution only. Recently, a first step toward such understanding was provided by a spectroscopic monitoring of the pulsating post-AGB star SAO 96709 (Lèbre et al. 1996). The line profile characteristics and velocity variations can be attributed to complex atmospheric motions and propagation of shock waves driven by the pulsations. In a preliminary analysis (Jeannin et al. 1996) based on linear and non-linear models, we could reproduce the main pulsation properties, namely the period and light curves, adopting the photospheric parameters inferred for this object and typical for post-AGB stars. The nonlinear models of Jeannin et al. (1996) also predict the development of pulsation-induced shock waves with amplitudes as high as 20 to 40 km.s^{-1} in the H_α line formation region. These results are in good agreement with the amplitudes deduced from the H_α emission in the present star (cf. Lèbre et al. 1996). A further check of consistency of the nonlinear models relies on the reconstruction of line profile as observed for C I and Ba II.

In the present paper we carry on our study of SAO 96709: namely, we examine the sensitivity of the dynamics and shock waves development to the initial parameters (mass, effective temperature, metallicity) and reconstruct the line profiles for carbone and barium. The basic observational data are recalled in Sect. 2. The nonlinear models and the analysis of the atmospheric structure and dynamics are described in Sect. 3 and 4. Section 5 is devoted to the line profile calculations and to the comparison with observed profiles. Special attention is paid to the different sources of line broadening and to the problem of turbulent motions in the atmospheres of post-AGB stars. Concluding remarks follow in Sect. 6.

2. Observations: present status

The high galactic latitude star SAO 96709 is identified as a variable F 5I supergiant presenting small and irregular variations of the magnitude $\Delta V \sim 0.15$ (Bogaert 1994). Parthasarathy et al. (1992) and Klochkova (1995) have derived for this object a metallicity [Fe/H]$= -1$, typical for Population II stars, with a strong excess in CNO and s-process elements. Finally, IR observations (Kwok et al. 1989; Bujarrabal 1992; Omont et al. 1995) indicate the presence of a dust envelope. All those properties support the classification of SAO 96709 as a post-AGB carbon rich star.

Spectroscopic observations performed by Lèbre et al. (1996) at the 1.52m telescope of the Observatoire de Haute-Provence show that the Ba II (5853.688 Å) and C I (6587.62 Å) lines are rather symmetric and synchroneous in radial velocity variation deduced from their Doppler shifts. The radial velocities indicate

pulsational motions with an amplitude of about 7.5 km.s^{-1}, and the period estimated is of the order of 30 days.

A comparison of the H_α profile with Kurucz's synthetic spectra of static atmospheres gives an effective temperature of the order of 5750 K, and a gravity $\log g \sim 0.5$. However, the observed H_α profiles are almost permanently seen in emission. The comparison with the Kurucz spectra should therefore be taken with caution. On the other hand, the observed H_α emission indicates the existence of shock waves with an amplitude of the order of 40 km.s^{-1} in the line formation region.

3. Nonlinear models

Hydrodynamical calculations are performed with a lagrangean code including time-dependent transfer of the continuous radiation, as described in Fokin (1990-1992). The shocks are treated implicitly by means of the von Newmann-Richtmeyer artificial viscosity in the Stellingwerf's form with the parameters (C_q,α)=(2.0,0.1). As already stressed in Jeannin et al. (1996), variation of C_q between 1 and 3 gives essentially the same pulsational characteristics and atmospheric dynamics. The OPAL Rosseland mean opacities of Rogers and Iglesias (1992) are adopted. We also examine the effect of using the previous Los Alamos opacities (LAOL). The results will be briefly summarized at the end of this section. Note that in principle, in the equation of the energy balance of the gas the use of the Planck mean opacity seems more logical (see Mihalas and Mihalas 1984) than Rosseland mean. However, as shows the detailed analysis, the effective opacity describing the radiative cooling of the matter (in the frequency-integrated form of this equation) is expected to be considerably lower than the Planck mean due to thermalization of the Lyman lines. Therefore, the use of the Planck mean would lead to an overestimation of the cooling rate. In a forthcoming paper we shall discuss this problem in more details.

In order to estimate the sensitivity of our results to initial conditions, we adopt various sets of basic parameters (mass, luminosity, effective temperature and composition). The choice is constrained to reproduce the observed period and magnitude variations, as well as the estimated properties of the shock waves. It must be also in agreement with estimations of the mass inferred by stellar evolution and with estimations of the effective temperature and surface density given by the obser vations. The detailed analysis will rely on the three following models:

Model A: M=0.8 $M_\odot$, L=5100 $L_\odot$, T=5750 K, X=0.7 and Z=0.01,

Model B: M=0.65 $M_\odot$, L=5120 $L_\odot$, T=5950 K, X=0.7 and Z=0.004,

Model C: M=0.65 $M_\odot$, L=5120 $L_\odot$, T=5950 K, X=0.7 and Z=0.001.

All calculations start with an initial model in radiative and hydrostatic equilibrium. Usually, about 300 cycles are needed to reach a limit cycle, with a typical limiting kinetic energy of the order of $E_k = 10^{41}$ erg. In each case we additionally checked the stability of E_k by increasing the integration time up to about 1000 cycles. Note, however, that for models which

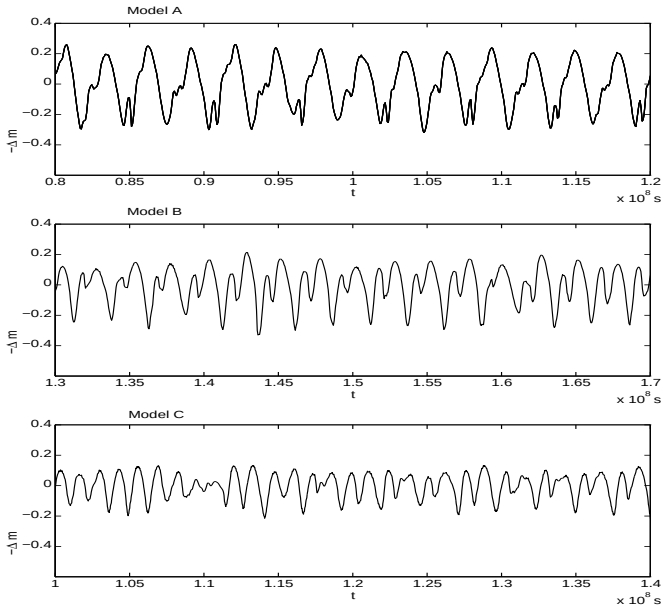

Fig. 1. Theoretical light curves for models A, B and C (see text)

are not strictly periodic (see Fig. 1), one can never ascertain that an attractor is reached since the convergency can be very slow.

Fig. 2 displays the Fourier spectra of the theoretical light curves of the three adopted models. The comparison with the LNA periods (see Jeannin et al. 1996 for more details) suggests that the model A is dominantly a first overtone pulsator. To confirm this point, we plot in Fig. 3 the amplitude and phase of the Fourier transform of $\Delta R/R$ for the three main peaks of the Fourier spectrum versus the stellar radius. The similarity of the nonlinear amplitude distribution of the main peak with the linear 1H eigenfunction of the radial displacement is clear enough.

The light curve of model B is slightly different from model A: the Fourier spectrum shows two peaks corresponding to the first and second overtones with a frequency ratio close to 1/2. A comparison of the Fourier transform of the nonlinear displacement with the LNA eigenfunctions suggests a coupling of the first and second overtones for this model.

The amplitude of model C (about 0.2 mag) gives the best agreement to the photometric observations of Bogaert (1994) ($\Delta v \sim 0.15$ mag). As in model B, the two overtones (first and second) are excited (Fig. 2), but the magnitude variations are more chaotic (Fig. 1).

The amplitudes of models A and B are slightly higher compared to the observed light curves. We believe that this property can be attributed to the larger Z, which leads to higher excitation rate due to increased opacity near the iron bump.

Finally, we have tested the effect of the Los Alamos opacities, which are substantially smaller compared to the improved set of OPAL, mainly in the region of the iron peak. Models adopting the LAOL data show strongly chaotic behavior, without any dominant mode.

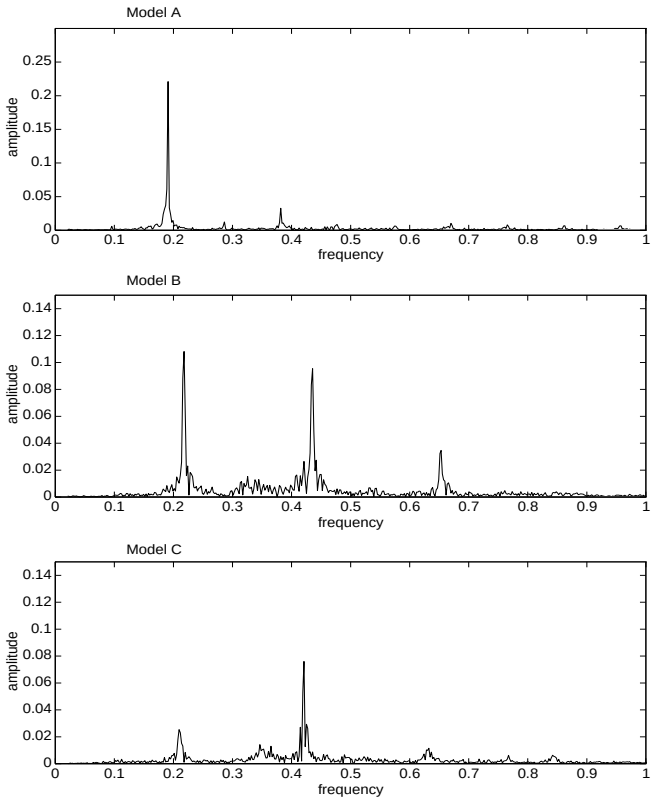

Fig. 2. Fourier amplitude spectra of magnitude variations for models A, B and C. The frequency is expressed in day^{-1}

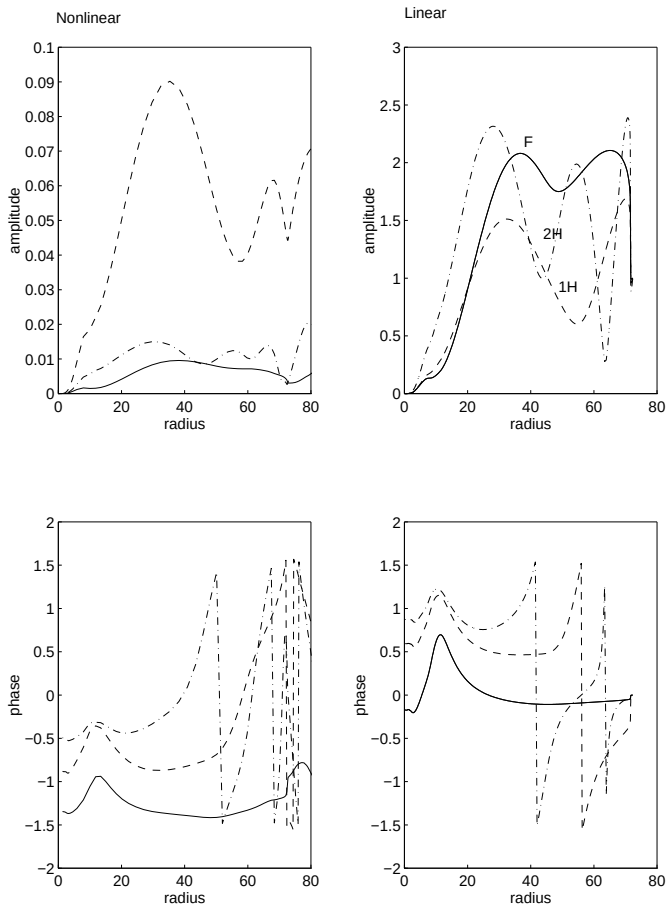

Fig. 3. Amplitude and phase of the Fourier transform of the non-linear relative variations of radius at the three main frequences (ν=0.0976 day^{-1}, ν =0.1966 day^{-1}, ν=0.3932 day^{-1}) obtained in the different mass zones versus the radius in solar units (left figures) for model A. These functions have to be compared with the linear lagrangean displacement eigenfunctions of the fondamental (solid line), the first harmonic (dashed line) and the second harmonic (dashdot line) (right figures)

4. Atmospheric structure

In this section, we analyse the dynamics of our model atmospheres. The mean photospheric radius of our models is about 70 $R_\odot$, with a radial amplitude variations of the order of 5 to 8 per cent. At the outer boundary of the models we use the condition of the homogeneous compression (in the Lagrangian frame). Numerically, it means that the density at the surface is C.V$_n$, where V$_n$ is the density in the middle of the outermost mass zone and C a constant lower than 1. In order to study the development of shock waves, we construct the models with an extented atmosphere (up to $\sim$ 90 $R_\odot$) with the density near the surface as low as 10^{-15}g. cm^{-3} .

No mass loss provoked by pulsation has been detected in our models, mainly due to small radial amplitude of pulsations. The radial velocity of the outer mass zones never exceed the escape velocity. However, as the dust formation has not been taken into consideration here, we are unable to make any conclusion about the real mass loss rate on the base of the present analysis.

We found several shock waves generated during each period, with different origin and strength. The generation and propagation of those shocks in the Eulerian frame are shown in Fig. 4, where the position of the maximum of artificial viscosity pressure is indicated, corresponding to the wave/shock fronts. The shock dynamics of the model A has already been described in our preceeding paper (Jeannin et al. 1996). We therefore briefly recall the main results. When the hydrogen recombination front (HRF hereafter) moves down as the star expands, it behaves like a "weak D-type" front (see Shu 1992, Fokin et al. 1996). When it stops at the end of the expansion phase, the velocity jump at the HRF gives rise to two running waves s3 and w3. The other mechanism of shock generation is related to the κ mechanism itself. At the maximum of compression the radiative energy is transformed into internal energy in the H ionization zone (due to the high increase of opacity), and is then restored, giving rise to a compression wave and, further, to s1. Both shocks s1 and s3 merge and give a shock with an amplitude of the order of 40 km.s^{-1} in the external layers of the model. The origin of the shock s2 remains unclear (cf. Jeannin et al. 1996) and seems to be due to the accumulation of several small amplitude compression waves. Its amplitude does not exceed 15 km.s^{-1}.

The dynamic motions of model B (Fig 5) are more complex. We find the same mechanism of generation of the shock s3

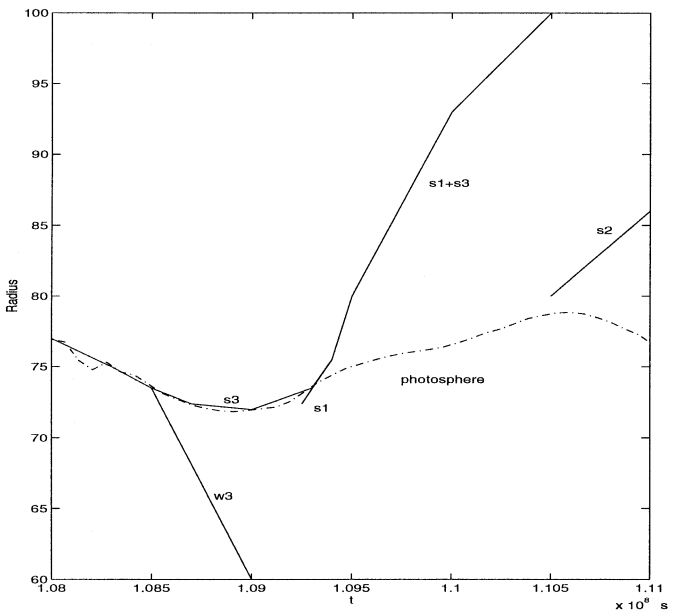

Fig. 4. Evolution of the shock waves in eulerian coordinates for model A (see text)

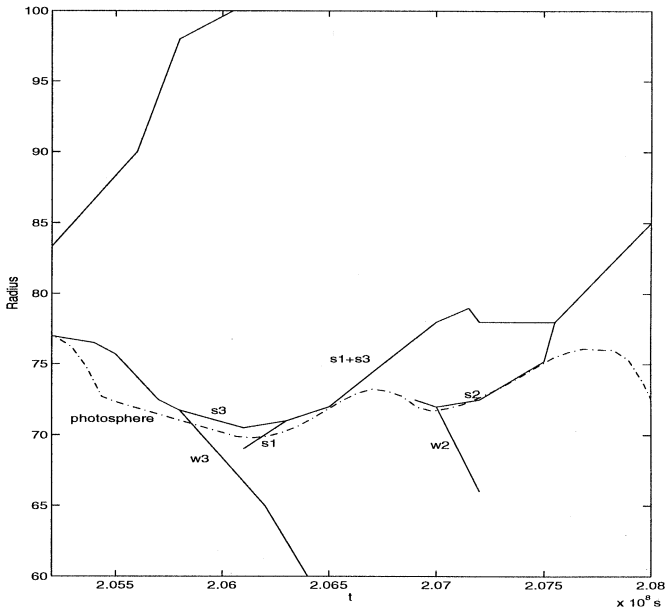

Fig. 5. Evolution of the shock waves in eulerian coordinates for model B (see text)

and the wave w3 (i.e. the stop of the recombination front at his maximum of penetration in the enveloppe of the star). The shock s1 is induced by compression wave due to κ-mechanism. The origin of shock s2 is however clear in this model: due to a coupling with the second harmonic, the HRF moves down twice in the lagrangean restframe during one pulsation period. As for s3 and w3, the stop of the HRF gives rise to two running waves propagating in opposite direction, w2 and s2. Finally, the shocks (s1+s3) and s2 merge in one main shock, whose amplitude does not exceed 40 km.s^{-1}.

Finally, in model C the shock waves formation is similar to those in models A and B , but they have smaller amplitude (of the order of 20 km.s^{-1}).

The results obtained from the three different models show that a variation of the basic parameters (mass, T_{eff}, L, Z) does not change the *qualitative* dynamic properties of the shock waves. Note that the amplitude of the shock waves of the order of 40 km.s^{-1} in the most external layers of models A and B are consistent with the shock waves interpretation of H_α observational profiles (Lèbre et al. 1996). The lower value found in model C may suggest that the metallicity adopted in this model is too low.

5. Metallic lines

5.1. Line profile modelling

The reconstruction of line profiles of C I and Ba II is based on the same code as used for Fe I lines by Fokin et al. (1996). The present calculations are made under the basic assumption of LTE, i.e. the source functions are always equal to the Planck function, and the ionization states are calculated from the Saha equation. Such a strong limitation may be justified by the fact that the lines of concern are rather faint and form near the photosphere where the density is high enough. One may then reasonably assume that collisional transitions dominate over the radiative ones and that Boltzmann statistic applies for the atomic populations.

Rotation is neglected in our calculations, since no observational evidences suggest that post-AGB stars have significant rotation velocity. This point is supported by evolutionary considerations, since the strong mass loss undergone during the previous phase of evolution, mainly during the AGB phase, results in angular momentum loss and reduction of the rotation speed.

5.2. Doppler shifts and line widths

We compute the Ba II and C I line profiles on the base of our non-linear grey atmosphere models, frozen at different pulsational phases. Thus the hydrodynamic modelling and the line profile analysis are performed here in a self-consistent manner with a minimum of free parameters. We stress that the comparison with the observed profiles should be regarded as qualitative, for the time resolution of the observations is rather low and does not allow at present any detailed analysis. In addition, the uncertainties inherent to post-AGB stars, namely the basic parameters (mass, L, T_{eff} etc.), restrict the problem to a general analysis of the most common features of those objects.

Regarding abundances, we first assume for carbone and barium the values deduced from the spectral analysis by Klochkova (1995). Although the Ba lines always remain deeper than the C ones, in agreement with the observations, the recommended values [Ba/Fe]= +1 and [C/Fe]= +1 lead to a significant discrepancies with the observed and predicted residual intensities. Better

agreement for the barium lines is reached with [Ba/Fe]=0, which is the mean observed abundance in stars with [Fe/H] $\sim$ -1 (cf. Mathews et al. 1992 for review), but is rather low compared to s-process enriched objects (MS, S and C stars). For the carbone lines a slighty better fit can be achieved with the C abundance 4 times higher than predicted. This value still remains compatible with determinations of abondances in C rich stars (Parthasarathy et al. 1992). We are aware of this point, but we do not expect the choice of the Ba or C abundance to affect our main conclusions, mainly concerning the effects of broadening (cf. next section). We finally adopt [Ba/Fe]=0 and [C/Fe]= +1.

Comparing the observed and theoretical amplitudes of the Doppler shifts of the C I and Ba II lines, a general agreement is found, considering the low time-resolution of the observed data (Fig. 6). However, the FWHM of the profiles, neglecting rotation and microturbulence, is systematically much smaller than the observed ones (Fig. 7). In order to explain such broadening by a velocity gradient effect, the velocity variation between the line core formation region and the photospheric region must permanently exceed 15 km.s^{-1}. On the other hand, the radial velocity amplitudes, deduced from the observed Doppler shifts of C I and Ba II lines (Fig. 6), are about of 7-8 km.s^{-1}. Provided that the radial velocity in the atmosphere is expected to change rather slowly with radius (in the absence of high amplitude shocks), such velocity gradient scenario should be rejected. Actually, as the detailed analysis of our hydrodynamical models shows, the velocity gradient in the relevant region does not exceed 7.5 km.s^{-1} at its maximum.

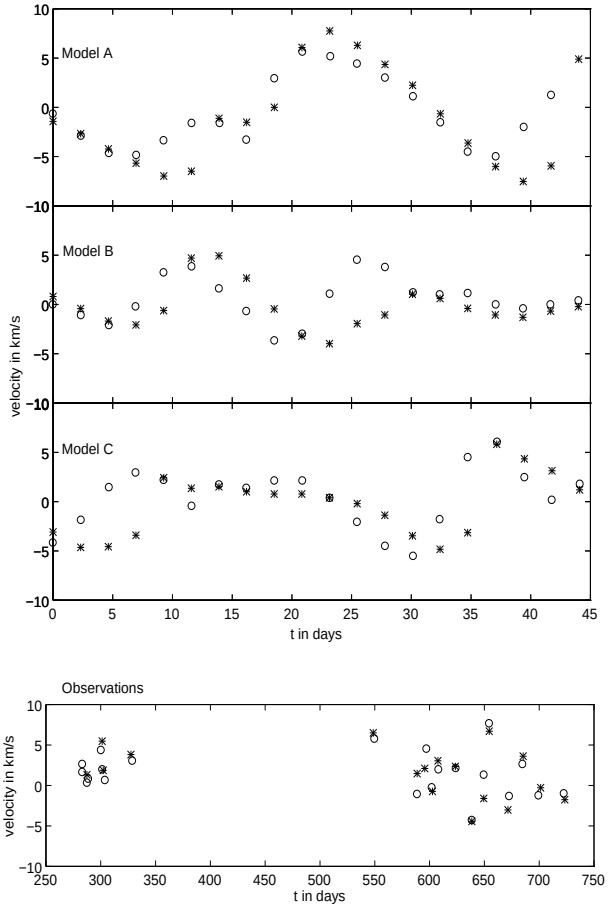

Fig. 6. Doppler shifts for the three models A, B and C (from upper to lower panel) and for the observation of Lèbre et al. (1996) (lower figure). The circles represent Doppler shifts of C I at 6587.62 Å, and the stars Doppler shifts of Ba II lines at 5853.688 Å

5.3. Sources of broadening

In order to analyse the discrepancy between the observed and predicted FWHM for the lines of concern, we check the effect of known atomic sources of broadening, such as *quadratic Stark effect* (using the prescription of Griem (1968)) and *Van der Waals effect* due to neutral hydrogen (using the prescription of Unsöld (1955)). We found that these sources affect by less than 5 per cent the FWHM values. This results is somewhat expected, since the atmosphere we are dealing with is rather cool and has very low density.

The presence of a *wind*, which may as well broaden the spectral lines, seems unlikely. Indeed, the most plausible mechanism of the wind from the late-type stars is the so-called dust-driven wind with the main acceleration taking place in the dust formation region, i.e relatively far from the photosphere (cf. Sedlmayr, 1989). It is therefore hard to connect the wind mechanism with strong velocity gradient near the photosphere, where the metallic lines of interest form. Moreover, the stellar center-of-mass velocity measurements based on radio molecular emission are in agreement with the mean photospheric velocity deduced from spectroscopic measurements, which seems to exclude the presence of any important wind.

Concerning *rotation*, as already mentioned, two effects act toward a reduction of rotation speed. On one hand, due to conservation of angular momentum as the star expands from the Main Sequence to the red giant branch the stellar rotation will considerably slow down. On the other hand, this effect is strengthened by the loss of angular momentum due to high mass loss during the Red Giant and AGB phases. We verify that the rotation in the theoretical models needed to explain the FWHM of the observed profile is of the order of 25 km.s^{-1} (Fig. 7). This value seems very high for evolved stars as post-AGB (cf. Gray, 1992). We therefore exclude the rotation as an important possible source of line broadening.

The non-LTE effects, neglected in the present work, can as well induce the line broadening. We expect, however, this effect to be small on the basis of the simplified analysis presented below. We performed several test calculations using a parametrized form of the source function $S = (1 - \beta).\bar{J} + \beta B$ typical for a two-level atom, where $\bar{J}$ is the scattering integral and B is the Planck function at the wavelength of the relevant line. The parameter β characterizes the influence of the bound-bound diffusion of photons on S. The case β =1 corresponds to complete LTE ($S = B$), while β =0 means complete diffusion in the line. The decrease of β from unity always leads mainly to a deepening of the line profile, while the FWHM hardly changes (less than 5 per cent). In addition, the lines in question form

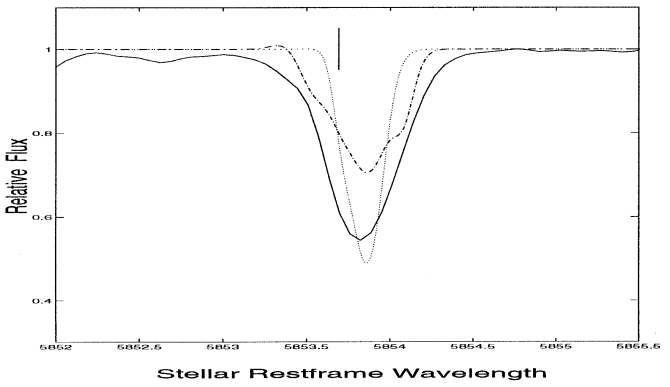

Fig. 7. Observed line profile (solid line), calculated line profiles of Ba II 5853.69 Å with rotation velocity of 25 km.s^{-1} (dashdot line) and calculated line profile without turbulence (dotted line). The observed profile is that of +367 d of Ba II spectrum in Lèbre et al. 1996

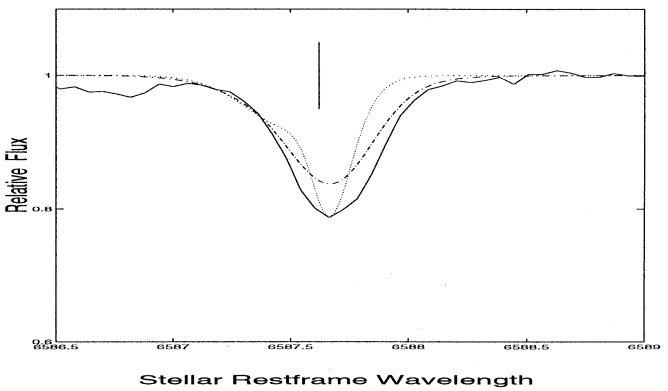

Fig. 8. Observed line profile (solid line), calculated line profile of C I 6587.63 Å with a turbulent velocity of 7.5 km.s^{-1} (dashdot line) and calculated line profile without turbulence (dotted line). The observed profile is that of +340 d of C I spectrum in Lèbre et al. 1996

rather deep, where the LTE condition can well be applied. We thus do not believe this mechanism to be very important.

The remaining (known) source of broadening is then the *turbulence*. It is well known that turbulent motions affect the FWHM of observed lines (Gray 1992). We assume that the effects of turbulence can be described as a local line broadening which adds to the thermal broadening. The local absorption profile is thus a Doppler profile with a width Δ_{tot} modified as $\Delta^2_{tot} = \Delta^2_{Dopp} + \Delta^2_{turb}$, with $\Delta_{turb} = U_{turb}\frac{\nu_o}{c}$. The microturbulent velocity U_{turb} is assumed constant all over the atmosphere. We found that the observed broadening can well be reproduced with U_{turb} as high as 4.5 to 8.5 km.s^{-1}. A general comparison between the theoretical and observed profiles is shown in Fig. 8 and 9. Though high, these values for the microturbulent velocity are in agreement with previous analysis of the line profiles of SA0 96709: Klochkova (1995), using the models of Kurucz, deduced a microturbulent velocity of $\sim$ 5.5 km.s^{-1}.

Fig. 10 shows the variations of the theoretical C I line profiles during one period. Unfortunately, we cannot compare in detail the observed and theoretical profiles without knowing the phase of the observations. Nevertheless, we show (Fig. 8 and 9) some good fits with the observed C I and Ba II line profiles for two selected phases. Note that one may expect the value of U_{turb} to vary during the pulsation period due to variable compression and shock waves induced by pulsation. The connection between pulsation and microturbulent velocity in the classical Cepheids have been studied by Fokin, Gillet and Breitfellner (1996) and Fokin and Gillet (1997). They put into evidence amplification of turbulence during the pulsation period, mainly due to a homogeneous compression of the atmosphere. For instance, in the classical Cepheids the turbulent velocity was found to vary from 2 to 7 km.s^{-1} during the period. Unfortunately, the lack of high-time resolution sets of observational profiles for the post-AGB stars does not allow any detailed estimation of the variations of U_{turb} with phase.

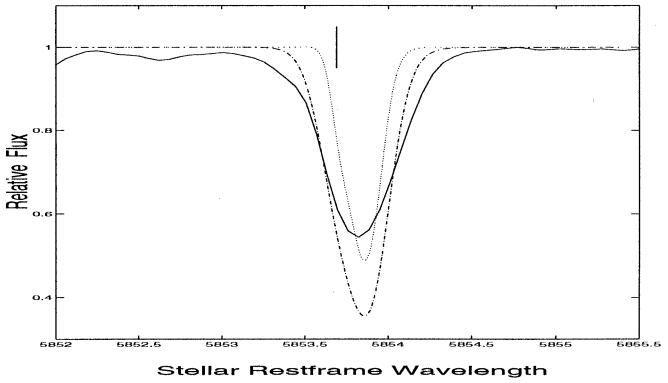

Fig. 9. Observed line profile (solid line), calculated line profiles of Ba II 5853.69 Å with a turbulent velocity of 5.5 km.s^{-1} (dashdot line) and calculated line profile without turbulence (dotted line). The observed profile is that of +367 d of Ba II spectrum in Lèbre et al. 1996

5.4. Discussion

Even if the present analysis is rather qualitative, it strongly suggests the presence of large turbulent motions near the photosphere of the post-AGB stars. These motions are expected to have a large spectrum of velocity, ignored in our present modelling. Indeed, we describe all the turbulence effects with a single empirical parameter, which characterises the smallest scales of turbulence, namely, microturbulence. This term is generally attributed to the turbulent motions characterised by eddies with length small compared to the length of the unit of the optical depth in the line. The eddies thus act like thermal motions of the atoms.

On the other hand, the large-scale turbulent motions, namely macroturbulence (see the solar granulation and supergranulation), imply that each vortex produces its own intensity spectrum contributing to the observed line profile (the size of the eddies being large compared to the length of the unit of the optical depth in the line). Thus the broadening effect of the macroturbulence is similar to that of a filter on the emergent

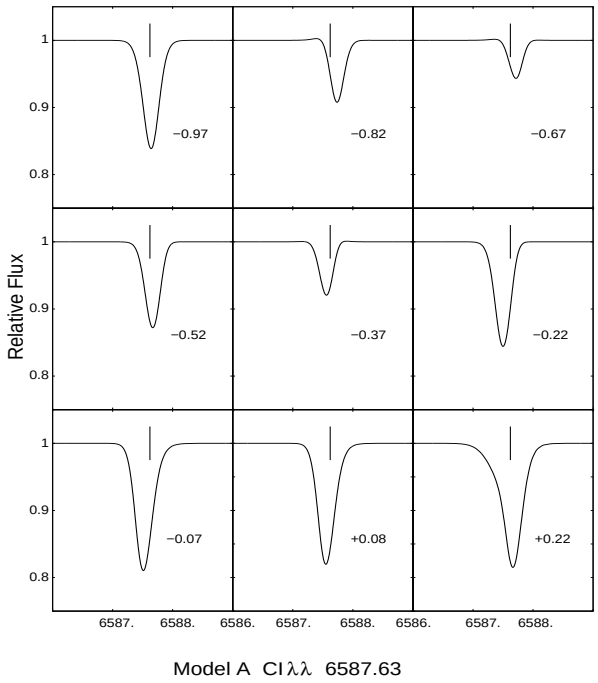

Fig. 10. Calculated line profiles of C I 6587.63 Å with a turbulent velocity of 5.5 km.s^{-1} during roughly one period (model A) in stellar restframe. The theoretical phase is indicated for each profile; the maximum of luminosity corresponds to the zero phase

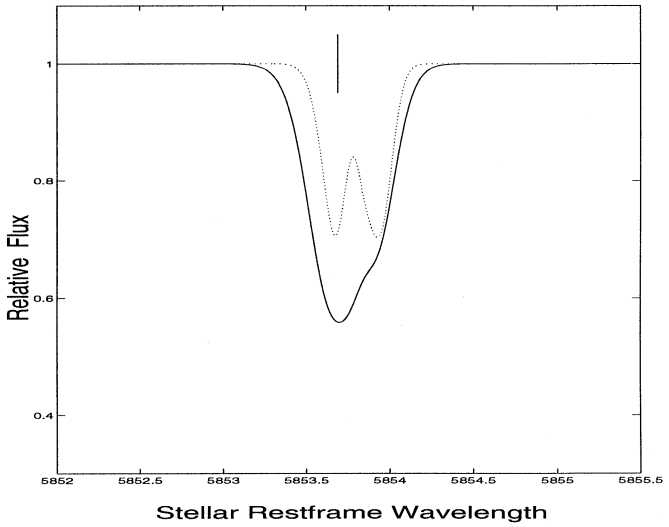

Fig. 11. Effect of turbulence on Schwarzschild doubling: a calculated Ba II line profile with turbulence 5.5 km.s^{-1} (solid line) and without turbulence (dashed line)

intensity which should be convoluted with a transfer function of the eddies (Gray 1988). Both turbulent effects are found to be important in luminous supergiants , though many points still remain unclear. Things are even more uncertain regarding the intermediate scale turbulence ("mesoturbulence"), which seems extremely difficult to include into the line profile calculations. We also note that the parameters of the turbulent motions should also depend on the height in the atmosphere, which makes the problem even more complex. Since there is presently no self-consistent description of turbulent motions, which takes into account its full scale spectrum, we restrict our analysis to the microturbulent motions being characterised by a lonely parameter. Since its numerical value is deduced from a fit with the observed FWHM, it is always (probably largely) overestimated, since at least a part of the observed broadening is due to the turbulent motions of a different scale, ignored in the present modelling. Keeping this in mind, one should take all the quantitative results obtained with a similar simplified approach with caution. Since the turbulent velocity found in the models is of the same order than the pulsational amplitude, one can expect a coupling between pulsation and turbulence, which can affect the pulsational motions in the atmosphere. But we must keep in mind that our turbulent velocity is just a parameter as explained above. At present we know very little about such a coupling due to the lack of a reliable theory.

In addition to the broadening effect, turbulent motions provoke a smoothening of the fine structure of the spectral lines. Actually, although hydrogen lines show evidences of shock waves in the atmospheres of post-AGB stars, the observed metal line profiles do not reveal any doubling due to Schwarzschild mechanism, but rather some assymmetry in their shape. One may suggest that the broadening of the line masks the doubling effect, as can be seen from Fig. 11 where this effect is illustrated for a theoretical line profile. We stress out that there is not enough observational data to ascertain that no Schwarzschild effect exists. However, if this point is confirmed by further more complete observations, it may confirm the presence of strong turbulent motions in these stars.

6. Conclusion

Following a preliminary hydrodynamical study of post-AGB stars (Jeannin et al. 1996), we devote the present work to a more complete understanding of these objects by means of spectral line analysis for different elements and comparison with available observed profiles. Our main results can be summarized as follow:

1) We confirm that the basic pulsation characteristics of post-AGB stars (i.e. period, light curve, velocity amplitudes) can be reproduced by nonlinear models based on fundamental parameters (mass, luminosity, T_{eff}) coherent with stellar evolution. We found that only the use of the new OPAL or OP opacities with improved metal absorption in the range $T \sim 2.10^5 K$ gives the observed quantities, with the main pulsation mode being the first overtone. The use of the LAOL opacities leads to a strongly chaotic behavior without any dominant mode.

2) We found shock waves with an amplitude of the order of 20 km.s^{-1} to 40 km.s^{-1} in the most external layers of our models. These waves have a much lower amplitude in the formation region of the metallic lines analysed here (see Fig. 6). These results are confirmed by the spectroscopic observations of Lèbre et al. (1996). We also predict that the broadening ef-

fect due to microturbulence can mask a line doubling due to the Schwarzschild mechanism.

3) The amplitude of the radial velocity, deduced from the theoretical line profiles for Ba II and C I, quantitatively agrees with the observed amplitude obtained by Lèbre et al. (1996). However, the lines computed without microturbulent motions are systematically narrower by 2-3 times. After all possible mechanisms of the line broadening being examined, we find that neither the velocity gradient in the line formation region nor the geometrical or non-LTE effects can provide the required broadening. The only plausible origin of the observed broadening is the turbulent motions with an average amplitude of 5-8 km.s^{-1}. Unfortunately, a detailed comparison with the observed profiles is not possible, due to their too low time resolution. This last point did not allow a study of the phase variations of microturbulence.

Further improved spectral observations with higher time resolution are highly needed to get more insight into the turbulent motions, structure and dynamics of these stars, as well as to clarify the details of their evolution.

Acknowledgements. We would like to thank N. Mauron and A. Lèbre for the valuable discussions. ABF also aknowledges the support of the Russian Foundation for the Fundamental Researches (grant 95-02-06359).

References

Aikawa T., 1991, ApJ, 374, 700
Aikawa T., 1993, ApJ, MNRAS, 262, 893
Bogaert, 1994, PhD. Univ. Louvain
Bujarrabal V., Alcolea J., planesas P., 1992, A&A 289, 429
Fokin A.B., 1990, ApSS, 164, 95
Fokin A.B., 1992, MNRAS, 256, 26
Fokin A.B., Gillet D., 1996, Breitfellner, M. G., A&A, 307, 503
Fokin A.B., Gillet D., 1997, A&A, in press
Gray D. F., 1988,*Lectures on Spectral-Line analysis: F, G, and K stars*, ed Arva, Ontario.
Gray D. F., 1992,*The observation and analysis of stellar atmospheres*, ed Cambridge Astrophysics Series
Griem H. R., 1968, Phys. Rev. 165, 258
Iben I. and Renzini A., 1983, Ann. Rev. Astron. Astrophys., 21, 271
Jeannin L., Fokin A.B., Gillet D., Baraffe I., 1996, A&A, 314,L1
Klochkova V.G., 1995, MNRAS 272, 710
Kwok S., Volk K., Hvrinak B. J., 1989, ApJ 346,265
Lèbre A., Mauron N., Gillet D., Barthès D., 1996, A&A, 310, 923
Mathews G.J., Bazan, G. Cowan J.J., 1992, ApJ, 391, 719
Mihalas D. and Mihalas B., 1984, *Foundations of Radiation Hydrodynamics*, ed Oxford Univ. Press, New York
Parthasarathy M., Garcia L.P., Pottasch S.R., 1992, A&A, 264, 159
Omont A., Moseley S.H., Cox P., Glacuum W., Casey S., Forveille T.,Kin-Wing Chan, Szczerba R., Loewenstein R.F., Harvey P.M, Kwok S., 1995, A&A, 454, 819
Rogers F.J., Iglesias, C.A. 1992, ApJS, 69, 495
Sedlmayr E. 1989, in: *From Miras to Planetary Nebulae: Which Paths for Stellar Evolution?*, ed. M.O. Mennessier and O. Omont, p. 179
Shu F.H., 1992, *The Physics of Astrophysics*, ed University Science Books
Unsöld A., 1955, *Physik der Sternatmosphären*, ed Springer-Verlag

This article was processed by the author using Springer-Verlag LaTeX A&A style file *L-AA* version 3.